

# Dynamics of a two-level system strongly coupled to a high-frequency quantum oscillator

E. K. Irish,<sup>1, 2, \*</sup> J. Gea-Banacloche,<sup>3</sup> I. Martin,<sup>4</sup> and K. C. Schwab<sup>2</sup>

<sup>1</sup>*Department of Physics and Astronomy, University of Rochester, Rochester, New York 14627*

<sup>2</sup>*Laboratory for Physical Sciences*

*8050 Greenmead Drive, College Park, Maryland 20740*

<sup>3</sup>*Department of Physics, University of Arkansas, Fayetteville, Arkansas 72701*

<sup>4</sup>*Theoretical Division, Los Alamos National Laboratory, Los Alamos, New Mexico 87545*

(Dated: December 2, 2024)

The advent of solid-state quantum devices offers new prospects for experimental study of the model consisting of a two-level system coupled to a quantum harmonic oscillator which has been studied primarily in the context of cavity quantum electrodynamics. Such devices may allow the exploration of new parameter regimes which are not well described by the near-resonance and weak-coupling assumptions of the rotating-wave approximation (RWA), necessitating the use and development of other theoretical tools. An adiabatic approximation is discussed which is valid when the dynamics of the oscillator occurs on a much faster time scale than that of the two-level system. Using this approximation, the time evolution of the occupation probability of the two-level system is calculated using both thermal- and coherent-state initial conditions for the oscillator, focusing particularly on collapse and revival phenomena. For thermal-state initial conditions parameter regimes are found in which collapse and revival regions may be clearly distinguished, differing significantly from the irregular evolution seen in the thermal-state RWA model. With coherent-state initial conditions the behavior is quite complex, exhibiting sensitive dependence on coupling strength and oscillator amplitude. One feature of the regime considered here is that closed-form evaluation of the time evolution may be carried out in the weak-coupling limit, which provides insight into the difference in the nature of the collapse function for thermal and coherent states. Finally, potential experimental observations in solid-state systems are discussed and found to be promising.

## I. INTRODUCTION

One of the simplest fully quantum-mechanical systems is that of a harmonic oscillator coupled to a two-level (spin-like) system. This problem has been studied for many years, and it has proved to be difficult to solve despite its apparent simplicity. Very early in its history Jaynes and Cummings<sup>1</sup> introduced what has come to be known as the rotating-wave approximation (RWA), which relies upon the assumptions of near-resonance and weak coupling between the two systems. The RWA has come into widespread usage partly because it allows the problem to be solved readily, and partly because it describes quite accurately the standard physical implementation of such a system: an atom coupled to a field mode of an electromagnetic cavity.<sup>2,3</sup> In this experimental situation, the coupling strength between the atom and the field is largely determined by the intrinsic dipole moment of the atom, and is thus constrained to be weak. The near-resonance condition is necessary if the two-level description of the atom is to be valid. Thus the RWA is a natural, and excellent, approximation in such a system.

Quantum-limited solid state devices are rapidly advancing to the point where they may offer an alternative to the traditional atom-cavity implementation of the spin-oscillator system. Recent experiments have shown clear spectroscopic evidence that a charge-based two-level system coupled to a superconducting transmission line behaves much like an atom in a cavity, and indeed the dipole coupling between the two systems is quite large compared to that achieved in atomic experiments.<sup>4</sup> Capacitive or inductive couplings offer the possibility of considerably larger coupling strengths than those possible with dipole coupling, even at large detunings between the fundamental frequencies of the oscillator and the two-level system. Some results have already been obtained for a flux-based, inductively-coupled system which give preliminary evidence for coupled quantum behavior and entanglement between the two-level system and the oscillator.<sup>5</sup> Another intriguing possibility involves capacitively coupling a charge-based two-level system to a nanomechanical resonator.<sup>6,7,8</sup> Such systems are capable of accessing coupling strengths and detunings far outside the regime in which the RWA is valid and thus different theoretical tools must be used to attack the problem.

In this paper we discuss an approximation which is able to treat strong coupling and large detuning. It is valid when the splitting frequency of the two-level system is much smaller than the frequency of the oscillator and holds well even for coupling strengths on the order of or larger than the oscillator frequency. The approximation is used to examine the time evolution of the two-level system when the harmonic oscillator begins in a thermally-occupied state or in a coherent state. Several effects of the coupling to the oscillator are distinguished, including enhanced apparent decoherence rates, frequency modification, and collapse and revivals of the Rabi oscillations. We will focus particularly on collapses and revivals in this model.

In the next section we introduce the form of the Hamiltonian to be considered and derive the adiabatic approximation. In Sec. III we evaluate the approximate time evolution of the two-level system coupled to, respectively, a Fock state, a thermal state, and a coherent state of the oscillator, and classify the behavior in several parameter regimes. Section IV contains a further approximation which allows evaluation in closed form of the infinite sums encountered in the thermal and coherent state models. The prospects for experimental observation of our predictions are analyzed in Sec. V. Section VI concludes the paper.

## II. ADIABATIC APPROXIMATION IN THE DISPLACED OSCILLATOR BASIS

The Hamiltonian which forms the basis for the calculations and discussion in this paper is

$$H = \frac{1}{2}\hbar\Omega\hat{\sigma}_x + \hbar\lambda\hat{\sigma}_z(\hat{a}^\dagger + \hat{a}) + \hbar\omega_0\hat{a}^\dagger\hat{a}, \quad (1)$$

taking  $\hat{\sigma}_z|\pm\rangle = \pm|\pm\rangle$ . This differs from the Hamiltonian typically considered in cavity quantum electrodynamics<sup>1,9</sup> (CQED) only by a rotation about  $\hat{\sigma}_y$ . The reason for taking this form is rooted in the particular solid-state system which we have in mind, consisting of a Cooper-pair box (CPB), or charge qubit, coupled to a nanomechanical resonator (NR). When the CPB is biased well away from its degeneracy point and is driven by a classical field resonant with its splitting frequency, an effective Hamiltonian may be found which has exactly the form of Eq. (1) (see Sec. V and the Appendix). The picture in this case is of the two-level system undergoing Rabi oscillations due to the external driving field which are then altered by the coupling to the oscillator, rather than the usual picture of the two-level system being driven by the oscillator. Although the Hamiltonian and therefore the results we obtain are not restricted to the CPB-NR system, we will use that language throughout most of the paper.

Some approximation is required in order to find an analytic solution to the problem. The most common approach is to assume that the two-level system and the oscillator are close to resonance,  $(\Omega - \omega_0) \ll \Omega, \omega_0$ , and that the coupling between them is weak,  $\lambda \ll \Omega, \omega_0$ . Then terms which do not conserve energy may be discarded (the RWA), resulting in what is usually termed the Jaynes-Cummings model (JCM).<sup>1,9</sup> As mentioned in the Introduction, this is an appropriate approximation for atom-cavity experiments; however, unlike atom-cavity systems, the solid-state system we are considering has the potential for strong coupling at large detunings. Therefore, in this paper we will treat the case in which the two-level system splitting frequency is much smaller than the oscillator frequency,  $\Omega \ll \omega_0$ , and the coupling strength is allowed to be large, perhaps even on the order of or larger than the oscillator frequency. The RWA is not appropriate in this limit.

An excellent way of treating this regime is via a type of adiabatic approximation. This approximation has been derived previously by several authors using different methods. Graham and Höhnerbach<sup>10,11,12</sup> refer to this regime as the “quasi-degenerate limit” and give the lowest-order expressions which we will derive. Schweber<sup>13</sup> utilized the Bargmann Hilbert-space representation and Crisp<sup>14</sup> solved recurrence relations; both these authors found higher-order corrections beyond what we present. The approach which we take is somewhat different. First, by neglecting the self-energy of the two-level system, we will derive the basis in which the rest of the calculation will be performed, called the “displaced oscillator basis.” In this basis the Hamiltonian may be truncated to a block diagonal form and the blocks solved individually, a process which is equivalent to introducing the two-level system self-energy only as needed to lift the degeneracy within individual subspaces in the displaced oscillator basis.

To begin with we consider eigenstates of the form  $|i, N_i\rangle = |i\rangle|N_i\rangle$  where  $|i = +, -\rangle$  denotes the eigenstates of  $\hat{\sigma}_z$  and  $|\phi_i\rangle$  are the corresponding oscillator eigenstates, found from the last two terms of Eq. (1) with  $\hat{\sigma}_z$  set to its eigenvalue of  $\pm 1$  as appropriate:

$$[\pm\hbar\lambda(\hat{a}^\dagger + \hat{a}) + \hbar\omega_0\hat{a}^\dagger\hat{a}]|\phi_\pm\rangle = E|\phi_\pm\rangle, \quad (2)$$

or, completing the square,

$$\left[ \left( \hat{a}^\dagger \pm \frac{\lambda}{\omega_0} \right) \left( \hat{a} \pm \frac{\lambda}{\omega_0} \right) \right] |\phi_\pm\rangle = \left( \frac{E}{\hbar\omega_0} + \frac{\lambda^2}{\omega_0^2} \right) |\phi_\pm\rangle. \quad (3)$$

Assuming  $\lambda/\omega_0$  to be real, the operator on the left-hand side may be rewritten as

$$\left[ \left( \hat{a}^\dagger \pm \frac{\lambda}{\omega_0} \right) \left( \hat{a} \pm \frac{\lambda}{\omega_0} \right) \right] = \hat{D}(\mp\lambda/\omega_0)\hat{a}^\dagger\hat{a}\hat{D}^\dagger(\mp\lambda/\omega_0), \quad (4)$$

where  $\hat{D}(\nu) = \exp[\nu(\hat{a}^\dagger - \hat{a})]$  is a displacement operator.<sup>15</sup> The operator in Eq. 4 may be interpreted as the number operator for a harmonic oscillator whose equilibrium position has been displaced by an amount  $\pm(\lambda/\omega_0)\Delta x_{ZP}$ .

Correspondingly, the eigenstates of this operator are displaced Fock (number) states,

$$|\phi_{\pm}\rangle = e^{\mp(\lambda/\omega_0)(\hat{a}^\dagger - \hat{a})} |N\rangle \equiv |N_{\pm}\rangle \quad N = 0, 1, 2, \dots \quad (5)$$

with energies given by

$$E_N = \hbar\omega_0 \left( N - \frac{\lambda^2}{\omega_0^2} \right). \quad (6)$$

These approximate eigenstates and energies constitute the “displaced oscillator” basis,<sup>14</sup> which will be used throughout the calculations.

This basis has a simple interpretation in the CPB-NR system. Due to the capacitive coupling, one charge state of the CPB will attract the NR and shift its equilibrium position closer to the CPB, while another charge state will repel the NR. As long as the stretching of the beam due to the attraction is small, the NR will remain approximately linear and may still be described as a harmonic oscillator. However, the position of the harmonic potential well will have moved. The displaced oscillator basis allows the use of the ordinary harmonic oscillator formalism within each displaced potential well. The correspondence of physical position displacement to the formal displacement operator makes this a natural basis to work in.

However, there are some peculiarities associated with using the displaced oscillator states as a basis. Although the states  $|+, N_+\rangle$  ( $|-, N_-\rangle$ ) form an orthonormal basis with  $\langle M_+ | N_+ \rangle = \delta_{MN}$  ( $\langle M_- | N_- \rangle = \delta_{MN}$ ), the states  $|N_+\rangle$  and  $|N_-\rangle$  are not mutually orthogonal. This may be understood easily in position space, where the displacement operator corresponds to a displacement in  $x$ . Consider, for example, the harmonic oscillator ground state  $|0\rangle$ , which has a Gaussian form: this state displaced by a finite amount is never completely orthogonal to the same state displaced by the opposite amount, although the displaced states may become very nearly orthogonal if the displacement is large enough. The overlap between Fock states displaced in different directions is given by

$$\langle M_- | N_+ \rangle = \begin{cases} e^{-2\lambda^2/\omega_0^2} (-2\lambda/\omega_0)^{M-N} \sqrt{N!/M!} L_N^{M-N}[(2\lambda/\omega_0)^2] & M \geq N \\ e^{-2\lambda^2/\omega_0^2} (2\lambda/\omega_0)^{N-M} \sqrt{M!/N!} L_M^{N-M}[(2\lambda/\omega_0)^2] & M < N, \end{cases} \quad (7)$$

where  $L_i^j$  is an associated Laguerre polynomial. Note that  $\langle M_- | N_+ \rangle = (-1)^{N-M} \langle N_- | M_+ \rangle$ . Together with the fact that  $\langle M_- | N_+ \rangle$  is real, this implies that  $\langle M_+ | N_- \rangle = (-1)^{M-N} \langle M_- | N_+ \rangle$ , which is a useful identity. The lack of orthogonality between different displacements leads directly to the unusual results in the two-level system dynamics which will be found later.

The next step is to reintroduce the two-level system self-energy,  $\Omega$ , which is assumed to be small. Reformulating the problem in terms of a matrix written in the displaced oscillator basis allows the approximation to be carried out in a natural way. Using the overlap functions calculated above, the matrix representing the Hamiltonian (1) may be written down:

where the order of the columns and rows is  $|+, 0_+\rangle, |-, 0_-\rangle, |+, 1_+\rangle, |-, 1_-\rangle, \dots$ . The approximation consists of truncating the matrix (8) to the block diagonal form

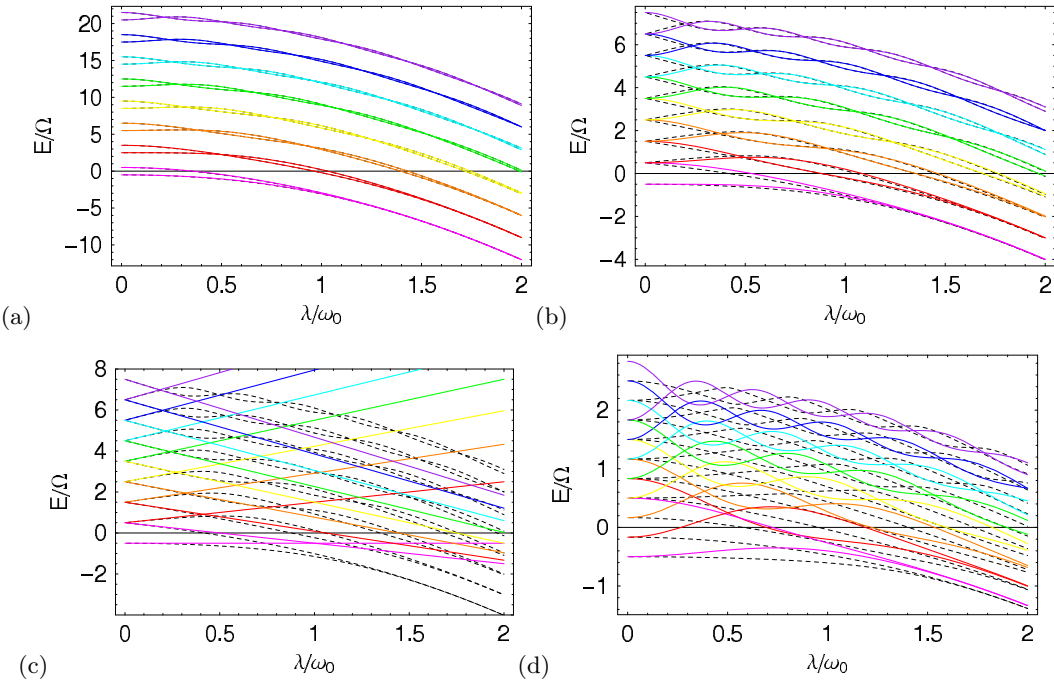


FIG. 1: Energy levels given by analytic approximation methods (solid lines) and by numerical solution of the full Hamiltonian (dashed lines). (a) Adiabatic approximation and numerical solution with  $\Omega/\omega_0 = 1/3$ . (b) Adiabatic approximation and numerical solution with  $\Omega/\omega_0 = 1$ . (c) Rotating wave approximation and numerical solution with  $\Omega/\omega_0 = 1$ . (d) Adiabatic approximation and numerical solution with  $\Omega/\omega_0 = 3$ .

In this approximation, the self-energy of the two-level system has been employed only where it is needed to lift the degeneracy of the displaced-oscillator basis states (Eqs. (5) and (6)). The natural interpretation of this form of the Hamiltonian is that the oscillator will be restricted to remain in the  $N_{\pm}$  subspace if it has been initialized in  $|N_+\rangle$  or  $|N_-\rangle$ . The degree of excitation of the oscillator does not change; only its equilibrium position changes. In this picture the condition  $\Omega \ll \omega_0$  may be seen as a statement about statics: the spacing of the oscillator energy levels is very large compared to the spacing of the two-level system, so a transition in the two-level system can never excite the oscillator. An alternative argument, found in Sec. III.C. of Ref. 16, is based on the separation of characteristic times in the two systems: given the assumption  $\Omega \ll \omega_0$ , the oscillator responds almost instantaneously to changes in  $\sigma_z$ , so the oscillator dynamics is “slaved” to the two-level system dynamics.

Due to its simple block diagonal form, Eq. (9) may be solved easily. The solutions in the  $N$ th block are given by

$$|\Psi_{\pm,N}\rangle = \frac{1}{\sqrt{2}}(|+,N_+\rangle \pm |-,N_-\rangle), \quad (10a)$$

$$E_{\pm,N} = \pm \frac{\Omega}{2} \langle N_- | N_+ \rangle + E_N. \quad (10b)$$

These energies and eigenstates constitute the adiabatic approximation to lowest order in  $\Omega/\omega_0$ .

Figure 1 shows the lowest-lying energy levels (10b) as a function of the coupling strength  $\lambda/\omega_0$  for different values of the ratio  $\Omega/\omega_0$ . For comparison purposes, the results of a numerical diagonalization of the full Hamiltonian (Eq. (1)) are also shown.

Consider first the case  $\Omega/\omega_0 = 1/3$ , shown in Fig. 1(a). This is within the regime in which we expect the approximate solution (10) to be valid. The “ripple” structure imposed by the Laguerre polynomials on the smooth variation of  $E$  with  $\lambda/\omega_0$  is immediately evident. This structure was noted in Ref. 14 and interpreted as an interference between states displaced in opposite directions. In the limit  $\lambda/\omega_0 \rightarrow \infty$  the distance between the wells becomes infinite, and the overlap  $\langle N_- | N_+ \rangle \rightarrow 0$ . With no mixing between the wells the spectrum becomes that of two identical harmonic oscillators and the energy levels become pairwise degenerate. The agreement with the numerical solution is excellent.

Another noteworthy feature of the structure of the energy levels is the multiple crossings which appear between pairs of levels. These are true crossings, not narrow avoided crossings, allowed by conservation of the parity operator  $\hat{P} = \exp[i\pi(\hat{a}^\dagger \hat{a} + \frac{1}{2} + \frac{1}{2}\hat{\sigma}_x)]$  in Eq. (1).<sup>10</sup> The approximate eigenstates (10a) are eigenstates of  $\hat{P}$ ; pairs of levels with different eigenvalues of  $\hat{P}$  are allowed to cross.

Figure 1(b) shows the resonance case,  $\Omega/\omega_0 = 1$ . Plots for this case also appear in Ref. 11. Interestingly, the agreement between the approximate solution and the numerical solution is still quite good, especially at larger coupling strengths. Compare this to the RWA energy levels,<sup>1</sup>  $E_{\pm,N}^{RWA} = N\hbar\omega_0 \pm \Omega/2 \pm \hbar\lambda\sqrt{N}$ , shown in Fig. 1(c). The RWA gives the correct limiting behavior as  $\lambda/\omega_0 \rightarrow 0$ , but diverges from the numerical solution starting around the point where the paired levels first cross. This comparison illustrates the dependence of the RWA upon the assumption of weak coupling, even when the oscillator and two-level system are exactly resonant.

Finally, Fig. 1(d) shows the case  $\Omega/\omega_0 = 3$ , which is out of the regime in which the adiabatic approximation is expected to hold. Plots of this case are given in Ref. 10; however, the approximate and numerical solutions are shown in different figures, making it difficult to compare the two. Our plot demonstrates that the adiabatic approximation breaks down in this regime except in the broadest qualitative sense. As soon as  $\Omega/\omega_0 > 1$  spurious level crossings appear at small values of  $\lambda/\omega_0$ , and a substantial phase difference begins to develop between the ripples in the numerical and approximate solutions. Clearly the adiabatic approximation discussed here is not a reasonable treatment for  $\Omega/\omega_0 > 1$ .

The displaced oscillator basis provides a physically intuitive picture for the derivation of an adiabatic approximation in the regime  $\Omega/\omega_0 \leq 1$ . Comparing the adiabatic approximation with a numerical solution shows that the approximation works quite well in the regime for which it was derived. Although this approximation has been derived previously, no authors seem to have explored its consequences for experimental observables. Much of the remainder of this paper will be devoted to a study of those consequences.

### III. DYNAMICAL BEHAVIOR

For applications in real systems, it is the dynamical behavior of the two-level system which we are particularly interested in. In this section we will discuss the time dependence of the two-level system observable  $\hat{\sigma}_z$ , which corresponds to charge in a Cooper-pair box. We will consider three commonly used states as initial conditions for the harmonic oscillator: the Fock state, the thermal state, and the coherent state, each of which may be applicable in different situations. As might be expected, the behavior of the two-level system changes dramatically depending on the initial oscillator state. We have verified the behavior obtained in the adiabatic approximation against a numerical solution of the full Hamiltonian. Provided the ratio  $\omega_0/\Omega$  is made large enough, the agreement is excellent over the short time scales which are likely to be experimentally accessible; the value  $\omega_0/\Omega = 10$  gives quantitative agreement over several dozen periods of oscillation. Time evolution in the adiabatic approximation shows a rich variety of behavior which we will demonstrate and classify.

Throughout this section the quantity to be examined is the probability of obtaining  $|-\rangle$  as a function of time,  $P(-, t)$ . The initial state of the two-level system will be taken to be  $|-\rangle$ , and the initial state of the oscillator will be given in the displaced basis corresponding to the state  $|-\rangle$ . This situation might be obtained, for example, by turning on the bias voltage  $V_g$  between the NR and the CPB, tuning the CPB gate bias voltage  $V_b$  so that the net bias is away from the degeneracy point, and allowing the CPB to relax to its ground state. Preparation of the oscillator state would vary depending on the type of state (Fock, thermal, or coherent); some indication of how each state might be prepared will be given when it is discussed. At time  $t = 0$  the microwave field is switched on and the system begins to evolve in time. Other initialization schemes might be imagined, but starting the oscillator in the displaced basis simplifies the mathematics.

An important point to keep in mind when comparing the results presented here with results from the JCM is that they are measured in a different basis relative to the Hamiltonian. The state  $|-\rangle$  is an eigenstate of the two-level-system operator  $\hat{\sigma}_z$  which is associated with the interaction term of the Hamiltonian. In the JCM the initial state and the measured state of the atom are chosen to be eigenstates of the bare atomic Hamiltonian rather than the interaction Hamiltonian. These are natural choices for the corresponding physical systems, but a degree of caution must be used in comparing the two models.

The simplest dynamical behavior is obtained when the oscillator begins in a displaced Fock state, such that  $|\psi(0)\rangle = |-\rangle \otimes |N_-\rangle$ . The time evolution of the probability to find the two-level system in the initial state is given by

$$\begin{aligned} P(-, t) &= |\langle -, N_- | \psi(t) \rangle|^2 \\ &= \cos^2(\Omega'^{(N)} t/2), \end{aligned} \tag{11}$$

where

$$\Omega'^{(N)} = \Omega \langle N_- | N_+ \rangle = \Omega e^{-2\lambda^2/\omega_0^2} L_N[(2\lambda/\omega_0)^2]. \tag{12}$$

The CPB undergoes Rabi oscillations (due to the external driving field), but with a frequency which is modified by the strength of the coupling to the resonator; following Ref. 16 we will refer to this as “adiabatic renormalization”<sup>30</sup>. The

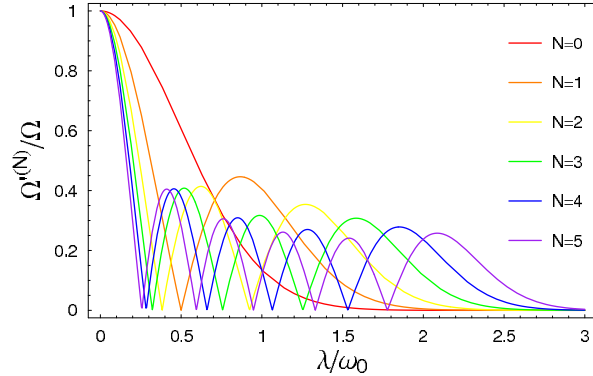


FIG. 2: Renormalized frequencies given by Eq. (12) for values of  $N = 0, 1, \dots, 5$ .

renormalized frequencies (12) are plotted versus the coupling strength  $\lambda/\omega_0$  in Fig. 2 for small values of  $N$ . Unlike the Rabi frequencies obtained in the JCM, the frequencies obtained here are not monotonic functions of the coupling strength  $\lambda$  or of  $N$  for  $N > 0$ .

One perhaps unexpected feature of these frequencies is the zeros which occur as the coupling strength increases. Comparison with numerical solution of the full Hamiltonian shows that the adiabatic approximation breaks down to some extent around the “critical points” in the coupling strength at which the renormalized Rabi frequency goes to zero. This point is discussed in Ref. 14, and a higher-order formula is derived which is valid even near the critical points. Some caution must be used in making predictions from our lowest-order formula for Fock state initial conditions. However, Fock states are highly non-classical states and although some methods for preparing such states in NRs have been proposed,<sup>8,17</sup> the experiments appear difficult. This paper is primarily concerned with time evolution from more realistic initial states, which involve some distribution of number states. The distribution reduces the contribution from any given number state, and our numerical studies indicate that the approximation works well even when states are included which have critical points near a given coupling strength.

The next initial condition for the oscillator which we will consider is a thermally-occupied state, sometimes also referred to as a chaotic state, in the displaced basis. This type of state is expected for an oscillator in thermal equilibrium with its environment, such as the NRs studied in the recent experiments of LaHaye *et al.*<sup>18</sup> The thermal state is a fully mixed state which must be described by a density matrix rather than a state vector. The two-level system is again taken to be initialized in the state  $|-\rangle$ , so that the initial density matrix for the coupled system is given by

$$\rho_{th}(0) = |-\rangle\langle-| \otimes \sum_N p_{th}(N) |N-\rangle\langle N-|, \quad (13)$$

where

$$p_{th}(N) = \frac{1}{(1 + \langle N \rangle)(1 + 1/\langle N \rangle)^N} \quad (14)$$

and  $\langle N \rangle = (e^{\hbar\omega_0/k_B T} - 1)^{-1}$  is the average number of quanta in the oscillator at the temperature  $T$ .

Assuming that system is weakly coupled to the thermal environment so that the influence of the environment is restricted to determining  $\langle N \rangle$ , the time evolution of the system is given by

$$\begin{aligned} \rho_{th}(t) &= e^{-iHt/\hbar} \rho_{th}(0) e^{iHt/\hbar} \\ &= \sum_N p_{th}(N) [\cos^2(\Omega'(N)t/2) |-, N-\rangle\langle -, N-| + \sin^2(\Omega'(N)t/2) |+, N+\rangle\langle +, N+| \\ &\quad + i \sin(\Omega'(N)t/2) \cos(\Omega'(N)t/2) (|-, N-\rangle\langle +, N+| - |+, N+\rangle\langle -, N-|)]. \end{aligned}$$

The reduced density matrix for the CPB is obtained by tracing over the oscillator states:

$$\begin{aligned} \rho_{th}^{CPB}(t) &= \sum_N p_{th}(N) [\cos^2(\Omega'(N)t/2) |-\rangle\langle-| + \sin^2(\Omega'(N)t/2) |+\rangle\langle+| \\ &\quad + i \sin(\Omega'(N)t/2) \cos(\Omega'(N)t/2) \langle N-| N_+ \rangle (|-\rangle\langle+| - |+\rangle\langle-|)]. \end{aligned} \quad (15)$$

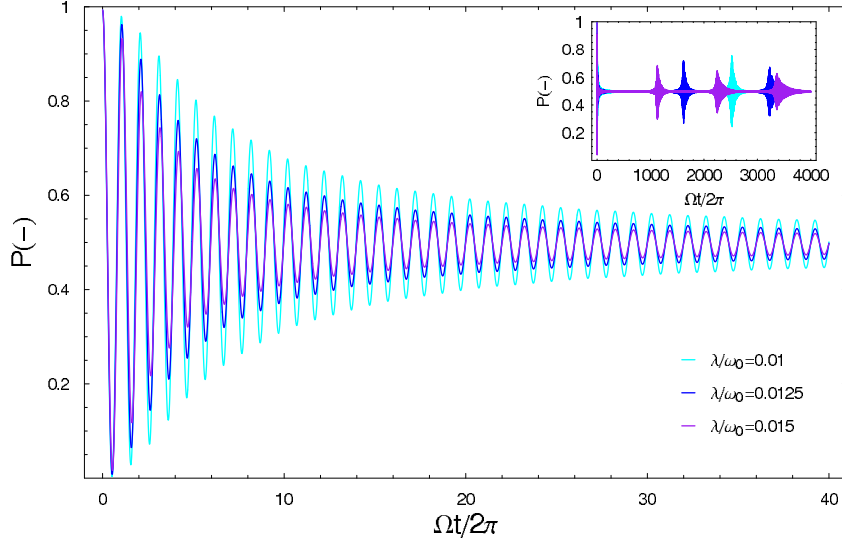


FIG. 3: Behavior of the two-level-system occupation probability in the high-temperature ( $\langle N \rangle = 100$ ), weak-coupling regime for short times (main figure) and long times (inset). Throughout the paper all time-dependent plots have  $\Omega/\omega_0 = 1/10$ .

From the reduced density matrix the probability of obtaining the state  $|-\rangle$  is found to be

$$\begin{aligned} P_{th}(-, t) &= \langle - | \rho_{th}^{CPB}(t) | - \rangle \\ &= \sum_N p_{th}(N) \cos^2(\Omega'^{(N)} t / 2). \end{aligned} \quad (16)$$

If no further approximations are made, the sum in Eq. (16) requires numerical evaluation. The parameter space is complicated, but at least three qualitatively distinct regimes of behavior may be found, characterized by the oscillator temperature and the coupling strength. In the very low temperature regime,  $\langle N \rangle \sim 0.01$ , the behavior consists of ordinary Rabi oscillations with a frequency renormalized by the coupling to the ground state of the oscillator. This renormalization becomes significant for relatively large coupling strengths,  $\lambda/\omega_0 \sim 0.1 - 1$ .

However, due to the large width in  $N$  of the thermal distribution the different frequencies  $\Omega'^{(N)}$  involved in the time series (16) tend to interfere with each other, producing a decay in the amplitude of the oscillations. This effect, known as a “collapse” in quantum optics,<sup>19,20</sup> dominates the short-time behavior at higher temperatures as long as  $\lambda/\omega_0$  is not too large. At longer times, the discrete nature of the spectrum allows a partial rephasing of the oscillations at different frequencies, resulting in “revivals” of the oscillation amplitude.<sup>20</sup> These behaviors are illustrated in Fig. 3. Several features are worth noting. First is the nonzero amplitude in the collapse region; this residual amplitude decreases with increasing temperature. Second, the collapse time and the times at which the revivals occur depend on the coupling strength: both the collapse time and the revival time shorten as the coupling strength increases. Finally, the amplitude of the revivals decreases and their width increases as time goes on, as the rephasing becomes less complete. Some of these features can be understood from a simple analytical approximation that will be introduced in the next section.

As the coupling strength is increased at a given temperature the behavior of the two-level system becomes increasingly erratic. Shorter revival times cause successive revivals to overlap and interfere so that the time evolution appears irregular. The coupling strength at which irregularity emerges is closely tied to the temperature: the higher the temperature, the smaller the coupling strength needed to produce irregular behavior. Higher temperature also results in decreased revival amplitude due to the larger number of frequencies in the sum, which causes the rephasing to be less complete. However, a signature of the revivals persists as a return to the bare Rabi frequency even at temperatures high enough that the behavior looks random and the revival amplitude is essentially washed out. Figure 4 illustrates the lapse into quasichaos and the persistent revival signature.

The variation of behavior from frequency renormalization to distinct collapse and revival dynamics to apparent randomness in the adiabatic approximation contrasts with the findings of Knight and Radmore,<sup>21</sup> who studied the time evolution of a two-level system coupled to a thermal oscillator state in the JCM. Although they distinguish collapse and revival regions, the behavior within those regions appears erratic, reminiscent of that found above for large coupling strengths. Clear and well-defined revival pulses do not occur in the JCM for any parameter values if the oscillator begins in a thermal state. In fact, the shape of the time-evolution curve is invariant in the JCM,

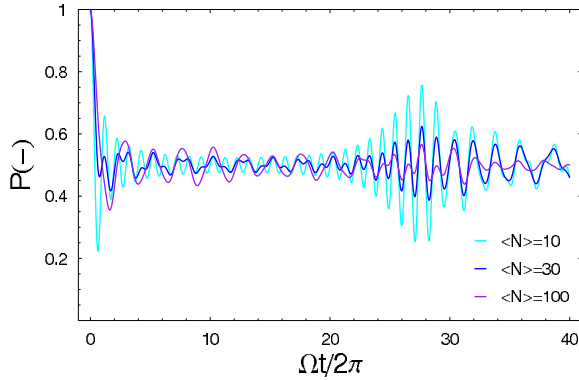


FIG. 4: Behavior of the first revival region as a function of temperature, with  $\lambda/\omega_0 = 0.1$ .

although the time scale and amplitude may change. The distinct revival areas found in the adiabatic approximation for smaller coupling strengths more closely resemble those obtained in the coherent-state JCM.<sup>20,22</sup>

Finally we turn to the case in which the oscillator begins in a displaced coherent state. Coherent states are considered to be the quantum states which most closely approach the classical limit; it might be expected that a driven NR could approximate a coherent state if the external driving dominates thermal fluctuations. The initial condition for the coupled system may be written as the pure state

$$|\psi_{coh}(0)\rangle = |-\rangle \otimes e^{-|\alpha|^2/2} \sum_{N=0}^{\infty} \frac{\alpha^N}{(N!)^{1/2}} |N-\rangle, \quad (17)$$

where  $\alpha$  is the (complex) amplitude of the coherent state, and we will define  $\langle N \rangle = |\alpha|^2$ .

The time evolution of the corresponding density matrix  $\rho_{coh}(0) = |\psi_{coh}(0)\rangle\langle\psi_{coh}(0)|$  may be calculated in the same way as before, with the resulting time-dependent probability

$$P_{coh}(-, t) = \sum_{N=0}^{\infty} p_{coh}(N) \cos^2(\Omega'^{(N)} t/2), \quad (18)$$

where  $p_{coh}(N) = e^{-\langle N \rangle} \langle N \rangle^N / N!$ . Equation (18) has the same form as Eq. (16) with the weighting function for the thermal distribution replaced by the weighting function for the diagonal elements of the coherent state.

As before, the sum in Eq. (18) requires numerical evaluation if no further approximations are made. However, the qualitative behavior is more difficult to classify. The regime  $\langle N \rangle \sim 0.01$  behaves much like the same regime in the thermal case. Frequency renormalization is the dominant effect, visible for relatively large values of  $\lambda/\omega_0$ .

For values of  $\langle N \rangle \gtrsim 10$  and fairly small coupling strengths  $\lambda$ , collapses and revivals appear which look similar to those found in the JCM.<sup>20</sup> The collapses are complete, with virtually no residual amplitude compared to those found above for the thermal state. At small values of  $\langle N \rangle$  the coherent state does not have a great enough spread in frequencies to create a complete collapse, resulting in residual oscillations in the collapse region similar to those found in the thermal state. Figure 5 compares the coherent state behavior with the thermal state behavior. As in the thermal case, a simple analytic approximation that will be presented in the next section explains some of these features.

At larger coupling strengths, however, the behavior does not necessarily lapse into irregularity as in the thermal case. For large  $\langle N \rangle$ , some unexpected results occur as the coupling is increased. The explanation for this lies in the non-monotonic dependence of the modified Rabi frequencies  $\Omega'^{(N)}$  on both  $\lambda$  and  $N$ .  $\Omega'^{(N)}$  is plotted as a function of  $\lambda/\omega_0$  for several values of  $N$  in Fig. 6; the values are chosen from the coherent-state distribution with  $\langle N \rangle = 100$  (inset) in order to give a sense of how the spread in frequency corresponds to the distribution in  $N$ . A sampling of the behavior of  $P(-, t)$  for  $\langle N \rangle = 100$  is shown on the left-hand side of Fig. 7. The values of  $\lambda/\omega_0$  illustrated there are indicated by vertical lines in Fig. 6. Considering the coherent-state weighting function  $p_{coh}(N)$  as a function of frequency yields a Fourier-transform-like distribution  $p_{coh}(\Omega'^{(N)})$ , which gives the amplitude of each frequency in the sum  $P(-, t)$ . This weighted frequency distribution is plotted on the right-hand side of Fig. 7 for each time series.

At zero coupling strength the weighted frequency distribution consists of a delta function located at  $\Omega'^{(N)}/\Omega = 1$ . As the coupling strength is increased, the distribution shifts downward and spreads out into an approximately Gaussian shape, which results in well-defined collapse and revival regions [Fig. 7(a)]. When the coupling strength approaches the critical point for the center of the distribution, the function begins to fold back on itself, resulting in a very fast

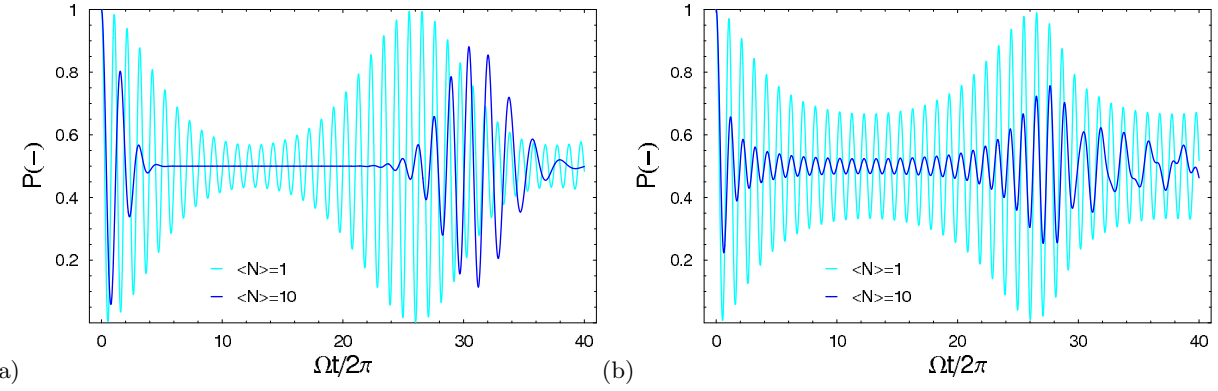


FIG. 5: Collapse and first revival for (a) coherent and (b) thermal states in a regime of regular behavior,  $\lambda/\omega_0 = 0.1$ . Unlike thermal states, coherent states cause complete collapses when  $\langle N \rangle$  is large enough.

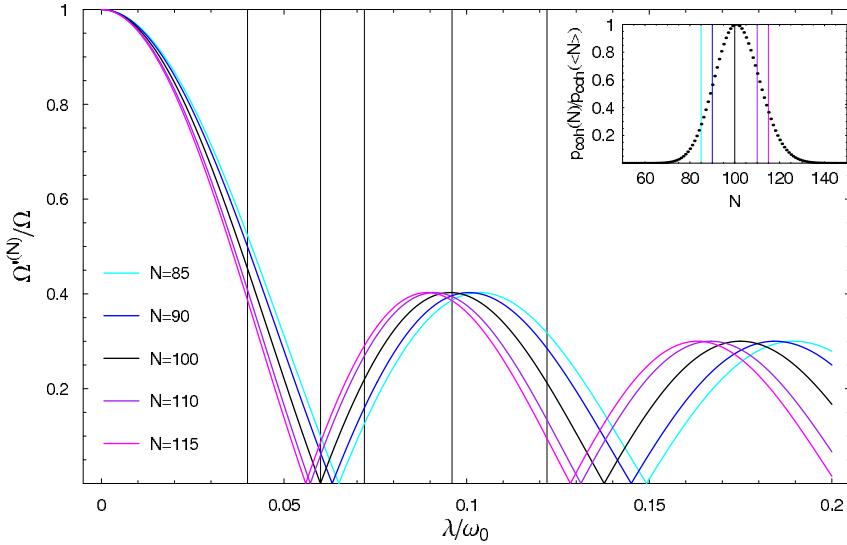


FIG. 6: Frequency renormalization as a function of coupling strength for some representative values of  $N$  from the coherent-state distribution with  $\langle N \rangle = 100$ . Vertical lines correspond to the coupling strengths used in Fig. 7. Inset: Normalized coherent-state probability distribution as a function of  $N$  with  $\langle N \rangle = 100$ . Vertical lines correspond to the values of  $N$  whose frequencies are plotted in the main figure.

collapse and strangely shaped revivals [Fig. 7(b)]. The distribution function then moves back to higher frequencies as the second “hump” of the renormalized frequency function  $\Omega'^{(N)}$  is traversed (Fig. 6), becoming almost Gaussian again. Correspondingly the time-dependent probability appears more regular [Fig. 7(c)]. At the peak of the second hump of  $\Omega'^{(N)}$  there is very little dispersion in the frequencies corresponding to different values of  $N$ , resulting in a nearly delta-function distribution and a very slow collapse [Fig. 7(d)]. The frequency distribution function then “bounces” back toward low frequencies. Deviations from a Gaussian distribution show up in the time-dependent probabilities as altered revival pulse shapes [Fig. 7(e)]. The behavior evolves between the samples shown here in a continuous manner, although in places it varies rapidly with  $\lambda/\omega_0$ .

The previous discussion demonstrates the complexity of the coherent-state adiabatic model. Somewhat unexpectedly, some of the phenomena seen above are blurred out at smaller values of  $\langle N \rangle$ . This may be understood by noting that two adjacent curves  $\Omega'^{(N)}$  and  $\Omega'^{(N+1)}$  diverge more strongly at small values of  $N$ : compare Figs. 2 and 6. Thus the weighted frequency distributions have a larger spread for smaller values of  $\langle N \rangle$  despite the fact that the coherent-state distribution is narrower in  $N$  for smaller  $\langle N \rangle$ . The wider spread in frequency space results in more erratic behavior, without the returns to regularity demonstrated in Fig. 7.

A similar analysis in frequency space also explains why the thermal-state model appears less complex. As a function of  $N$ , the maximum of the thermal state distribution is fixed at  $N = 0$  regardless of the value of  $\langle N \rangle$ , while the maximum of the coherent state distribution is given by  $\langle N \rangle$ . The frequency shift in the state  $N = 0$  is monotonic

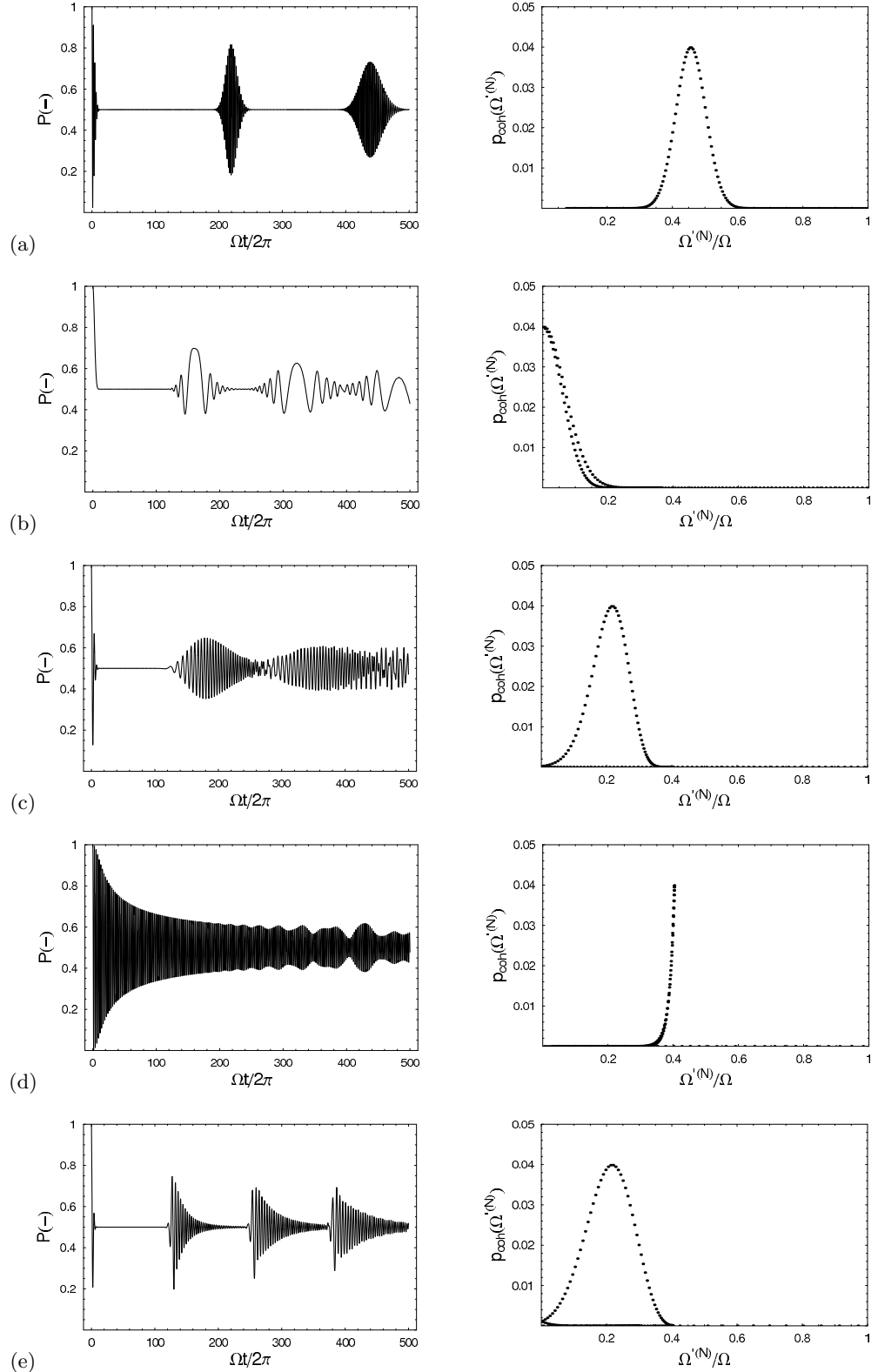


FIG. 7: Some of the strange types of behavior which appear in the coherent-state case with  $\langle N \rangle = 100$  and the weighted frequency distributions  $p_{coh}(\Omega'^{(N)})$  which lead to them. The coupling strengths used are  $\lambda/\omega_0$  = (a) 0.04, (b) 0.06, (c) 0.072, (d) 0.096, (e) 0.122.

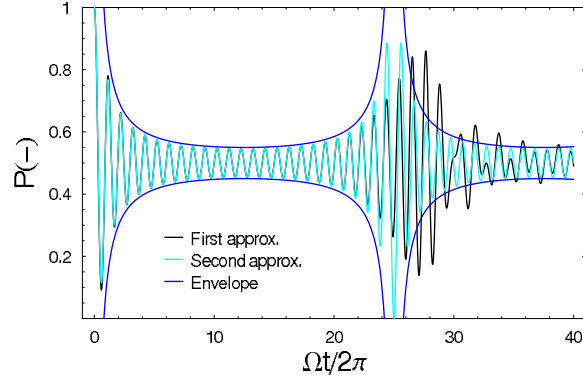


FIG. 8: Comparison of the first (adiabatic) approximation [Eq. (16)] and the second (weak coupling) approximation [Eq. (20)] for the thermal-state model. Also shown is the envelope function derived from Eq. (21) by neglecting the rapidly-oscillating factor  $\sin(\Omega t)$ . Parameters used are  $\langle N \rangle = 5$  and  $\lambda/\omega_0 = 0.1$ . Although these values are near the limit of validity of the approximations used, the agreement up to the first revival is excellent.

as a function of  $\lambda/\omega_0$  and slow compared to the shift for higher values of  $N$  [Fig. 2]. Thus the maximum of the weighted frequency distribution for the thermal state shifts less dramatically than the maximum of the frequency distribution for the coherent state, and the changes in the shape of the distribution are less pronounced.

Applying the frequency distribution function analysis to the JCM shows how the complicated dependence on  $N$  and  $\lambda$  of the frequencies  $\Omega'^{(N)}$  in the adiabatic approximation leads to a much richer variety of behavior than that found in the JCM. The Rabi frequencies in the JCM change monotonically with  $N$  and  $\lambda$  in such a way that the frequency distribution function changes in width but never in shape. Changes in  $\langle N \rangle$  and  $\lambda$  result in changes in the amplitude and time scale of the evolution; however, the shape of the evolution is unaltered. The large variation of behavior with  $\langle N \rangle$  and  $\lambda$  is a distinctive feature of the adiabatic approximation.

#### IV. THE WEAK COUPLING LIMIT

Although the adiabatic approximation allows evaluation of the time-dependent behavior of the two-level system, the results for thermal or coherent oscillator states are given by infinite sums which must be numerically evaluated. This is also true in the JCM, although integral approximation techniques have been used to derive some approximate analytic expressions.<sup>20,22</sup> An interesting feature of the adiabatic approximation is that taking the weak coupling limit allows closed-form evaluation of the time evolution for both thermal and coherent initial states.

For small values of  $(\lambda/\omega_0)^2$  the modified Rabi frequencies given in Eq. (12) may be approximated as<sup>23</sup>

$$\Omega'^{(N)} \approx \Omega[1 - (N + 1/2)(2\lambda/\omega_0)^2]. \quad (19)$$

This approximation enables the sums in Eqs. (16) and (18) to be carried out.<sup>23</sup> For the thermal state, Eq. (16) becomes

$$P_{th}(-, t) \approx \frac{1}{2} + \frac{1}{2} \frac{\cos(\Omega t) \cos[\Omega(2\lambda/\omega_0)^2 t/2] + (1 + 2\langle N \rangle) \sin(\Omega t) \sin[\Omega(2\lambda/\omega_0)^2 t/2]}{1 + 4\langle N \rangle (1 + \langle N \rangle) \sin^2[\Omega(2\lambda/\omega_0)^2 t/2]}. \quad (20)$$

A comparison of Eqs. (16) and (20) is shown in Fig. 8. It is apparent that even for relatively large values of  $\lambda/\omega_0$  the second approximation works quite well in the initial collapse region and captures the general qualitative behavior of the function. In the limit  $\langle N \rangle \gg 1$ , Eq. (20) reduces to

$$P_{th}(-, t) \approx \frac{1}{2} + \frac{\sin \Omega t}{4\langle N \rangle \sin[\Omega(2\lambda/\omega_0)^2 t/2]}. \quad (21)$$

From this formula some of the characteristics discussed in the previous section are immediately evident. Revivals occur when  $\Omega(2\lambda/\omega_0)^2 t/2 = \pi m$  for  $m = 1, 2, \dots$ , giving a revival time  $\tau_r = 2\pi/[\Omega(2\lambda/\omega_0)^2]$  which decreases with increasing  $\lambda/\omega_0$  as expected. The minimum oscillation amplitude in the collapse region scales as  $1/\langle N \rangle$ . However, Eq. (21) diverges as  $t \rightarrow 0$  as well as at the revival times, so it is not useful in predicting the shape of the collapse envelope at short times or the nature of the revival envelope function.

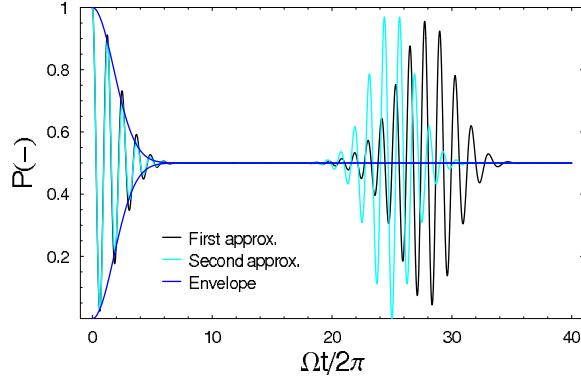


FIG. 9: As for Fig. 8, but for the coherent-state model; all parameters are identical. The envelope shown is the Gaussian collapse function given by Eq. (23) without the rapidly-oscillating cosine factor.

Within the weak-coupling approximation, the coherent-state evolution may be evaluated as well. Equation (18) yields the sum

$$P_{coh}(-, t) \approx \frac{1}{2} + \frac{1}{2}e^{-2\langle N \rangle \sin^2[\Omega(2\lambda/\omega_0)^2 t/2]} \cos\{\langle N \rangle \sin[\Omega(2\lambda/\omega_0)^2 t] - [1 - (2\lambda/\omega_0)^2/2]\Omega t\}, \quad (22)$$

which in the limit  $\Omega(2\lambda/\omega_0)^2 t \ll 1$  reduces to

$$P_{coh}(-, t) \approx \frac{1}{2} + \frac{1}{2}e^{-[\langle N \rangle \Omega^2(2\lambda/\omega_0)^4/2]t^2} \cos\{[(\langle N \rangle + \frac{1}{2})(2\lambda/\omega_0)^2 - 1]\Omega t\}. \quad (23)$$

The last form demonstrates the Gaussian collapse envelope at short times which is also found in the coherent-state JCM.<sup>19,20,22</sup> However, the full expression given in Eq. (22) is necessary in order to obtain revivals. Notice that the revival time  $\tau_r$  is the same as in the thermal case. A comparison of Eqs. (18) and (22) is shown in Fig. 9. As in the thermal state case, the second approximation works well in the initial collapse region.

This approximation highlights once again the role of the functional form of the modified Rabi frequencies (12) in controlling the time evolution. Rabi frequencies linear in  $N$  are obtained in a model similar to the JCM but involving three atomic levels and two photons.<sup>24</sup> Since all the frequencies involved are integer multiples of the bare Rabi frequency, the interfering oscillations rephase completely, leading to perfectly periodic, full-amplitude revivals for both coherent-state and thermal-state initial conditions. As demonstrated above, the renormalized Rabi frequencies in the adiabatic approximation are linear in  $N$  to first order. This is not the case in the usual two-level JCM, which yields Rabi frequencies which go as the square root of  $N$ . The closer approach to linearity in  $N$  explains why clear revivals may be found in the adiabatic model even for a thermal state, while the thermal-state JCM always produces erratic behavior.

## V. EXPERIMENTAL PROSPECTS

The primary requirement for experimental exploration of physics in the adiabatic regime is strong coupling at a large detuning between the two-level system and the harmonic oscillator. Atom-cavity systems typically have coupling strengths  $\lambda/\omega_0 \sim 10^{-6} - 10^{-7}$  at detunings of  $\Delta/\omega_0 \sim 10^{-5} - 10^{-7}$ , and are well described by the RWA.<sup>2,3</sup> The adiabatic regime requires numbers several orders of magnitude larger, which seems unlikely to be achieved with atoms. However, recent progress in solid-state systems suggests that experimental implementation of the model discussed here may be possible fairly soon. Already there is spectroscopic evidence that a system consisting of a CPB coupled to a superconducting transmission line has achieved the “strong-coupling limit” of CQED, in which coherent dynamics occurs faster than the decoherence rates.<sup>4</sup> The coupling strength obtained at zero detuning was  $\lambda/\omega_0 \sim 10^{-3}$ , which is a significant improvement over atomic systems. However, since the coupling is through the electric dipole moment it may be difficult to increase the coupling strength by the two orders of magnitude needed to get out of the RWA regime, and significant coupling at large detunings is unlikely.

Coupling strengths much larger than those possible with dipole coupling may be achieved with capacitive or inductive couplings. Some recent experimental results on a flux qubit inductively coupled to a superconducting quantum interference device (SQUID) that acts as both a measuring device and a quantum harmonic oscillator<sup>5</sup> appear very promising. Coherent oscillations in the qubit were observed with Rabi frequencies ranging up to around the qubit

splitting frequency. Since the oscillator frequency was about half the qubit splitting frequency, an analysis similar to that given below for the CPB-NR system yields values of  $\Omega/\omega_0 \lesssim 2$ . Given the coupling strength of  $\lambda/\omega_0 \sim 0.1$ , the adiabatic regime is already within the reach of this system.

Although it has not yet been demonstrated, the system consisting of a CPB capacitively coupled to a NR appears to be another potential candidate for achieving the adiabatic regime. The remainder of this section will be devoted to an analysis of the circumstances under which this would be possible.

The Hamiltonian is given by<sup>8</sup>

$$H_{TOTAL} = H_{CPB} + H_{NR} + H_{int} \quad (24)$$

$$H_{CPB} = 4E_C(n_g - \frac{1}{2})\hat{\sigma}_z - \frac{1}{2}E_J\hat{\sigma}_x \quad (25)$$

$$H_{NR} = \hbar\omega_0\hat{a}^\dagger\hat{a} \quad (26)$$

$$H_{int} = \hbar\lambda(\hat{a}^\dagger + \hat{a})\hat{\sigma}_z, \quad (27)$$

where  $\hat{a}^\dagger, \hat{a}$  are harmonic-oscillator raising and lowering operators which act on the NR;  $\hat{\sigma}_z, \hat{\sigma}_x$  are Pauli spin matrices operating in the charge basis of the CPB;  $n_g = (C_b V_b + C_g V_g)/2e$  where  $C_b$  and  $V_b$  are the CPB biasing capacitance and voltage and  $C_g$  and  $V_g$  are the capacitance and voltage between the NR and the CPB;  $E_C$  and  $E_J$  are the Coulomb and Josephson energies;  $\omega_0$  is the NR oscillator frequency in the absence of coupling; and  $\lambda = -4E_C n_g^{NR} \Delta x_{ZP} / \hbar d$  where  $n_g^{NR} = C_g V_g / 2e$ ,  $\Delta x_{ZP} = \sqrt{\hbar/2m\omega_0}$ , which is the zero-point position uncertainty of the NR ground state, and  $d$  is the distance between the NR and the CPB.

One way of reducing this Hamiltonian to the form of Eq. (1) is to bias the Cooper-pair box to the degeneracy point, where  $n_g = 1/2$ . However, typical values of  $E_J/h$  are on the order of several GHz, whereas the highest reported nanomechanical resonator frequency is about 1 GHz.<sup>25</sup> The approximation we have derived in this paper is based on the assumption that the effective splitting frequency of the two-level system is much smaller than the frequency of the oscillator,  $\Omega \ll \omega_0$ , which would be difficult to satisfy for degeneracy-point biasing.

However, an effective Hamiltonian of the correct form which satisfies the condition  $\Omega \ll \omega_0$  may be found given a few reasonable assumptions. Physically, this involves biasing the CPB well away from degeneracy so that  $4E_C(n_g - 1/2) \gg E_J/2$  and applying an oscillating voltage to the CPB bias gate, a procedure which is used in performing spectroscopy.<sup>26</sup> Assuming that the frequency of the oscillating voltage is equal to the splitting frequency of the box and that the amplitude of the oscillating voltage is small, the Hamiltonian may be approximated by Eq. (1) with  $\Omega = 8gE_JE_C(1/2 - n_g)/\{[8E_C(1/2 - n_g)]^2 + E_J^2\}$ , where  $g = 4E_C C_b V_b^{ac} / 2e\hbar$  is the Rabi frequency induced by the oscillating voltage. The Appendix contains a detailed derivation of this approximation.

For this situation, the regime in which the adiabatic approximation is valid aligns well with current experimental parameters. Starting with a NR frequency<sup>25</sup>  $\omega_0/2\pi = 1$  GHz, taking  $\Omega/\omega_0 = 1/10$  requires an effective CPB Rabi frequency  $\Omega/2\pi = 100$  MHz. With CPB parameters  $E_C/h = 20$  GHz and  $E_J/h = 7$  GHz and a bias point such that  $n_g = 1/4$ , the Rabi frequency induced by the oscillating voltage should be about 0.5 GHz. Assuming a bias-gate capacitance of  $C_b = 10$  aF, the required amplitude for the oscillating voltage is  $V_b^{ac} = 0.2$  mV, which may be achieved easily. Note that these numbers also satisfy the requirements for derivation of the effective Hamiltonian which are given in the Appendix. Since the coupling is capacitive,  $\lambda/\omega_0$  is limited by how small the distance between the NR and the CPB island can be made and by how large a voltage may be applied without damage to the NR. Values on the order of  $10^{-2} - 1$  should be possible. These numbers appear to be well within the reach of present technology.

Unfortunately the dephasing times for coherent oscillations in a CPB which have been measured so far are quite short. Vion *et al.*<sup>27</sup> found a dephasing time of  $0.5\mu\text{s}$  at the degeneracy point. As the bias voltage is tuned away from the degeneracy point, the dephasing time drops rapidly,<sup>28</sup> which is attributed to low-frequency charge noise. In order to see the effects predicted here, coherence times of several effective Rabi periods, on the order of several tens of nanoseconds, would be necessary; this would require significant improvement over current experiments. However, charge noise is not believed to be intrinsic, and advances in materials and fabrication may reduce the problem.

## VI. CONCLUSION

The adiabatic approximation we have discussed in this paper provides a rich and robust framework for exploring spin-oscillator physics outside the rotating-wave approximation. Although it is derived under the assumption that the two-level splitting frequency  $\Omega$  is much smaller than the oscillator frequency  $\omega_0$ , it works well even when  $\Omega = \omega_0$ ; indeed, it provides a more accurate description at large coupling strengths than the RWA. The energy levels obtained from this model exhibit nonmonotonic dependence on the oscillator occupation number  $N$  and the coupling strength  $\lambda$ . This leads directly to complex time-dependent behavior of the two-level system, which may exhibit frequency

renormalization, collapse and revival of coherent oscillations, or irregularity. Such behavior is quite sensitive to the initial state of the oscillator and the coupling strength in some parameter regimes.

Although this approximation is not new, solid-state experiments currently underway provide motivation for a more thorough exploration of its consequences. The pursuit of quantum computing has catalyzed the development of new types of devices which act as artificial atoms. Given the success of atom-cavity experiments in demonstrating various characteristics of quantum behavior, it is not surprising that solid-state analogs are being pursued. However, such systems have the capability to reach regimes which are inaccessible to traditional atom-cavity systems, in which the RWA is no longer valid. This paper has demonstrated some of the complexity which may be encountered at large detuning and strong coupling.

In particular, we have chosen to focus on a charge-based two-level system coupled to a nanomechanical resonator. Observation of the two-level system may offer some insight into the quantum nature of the resonator, just as atoms provide a sensitive probe for the nonclassical nature of electromagnetic fields. At fairly high resonator temperatures, the shape of the collapse of the coherent oscillations in the CPB may provide some information about the distribution of NR states: a thermal state gives a different envelope function than a coherent state. For either distribution, the shift from collapse dynamics to frequency renormalization would be a clear indication of near-ground-state cooling of the resonator. Finally, the observation of revivals, which are a strictly nonclassical phenomenon, would give evidence for the quantum nature of a macroscopic mechanical object. Such experiments appear to be nearly within the reach of current technology.

### Acknowledgments

Helpful discussions with Keith Miller, Alex Hutchinson, Carlos Sanchez, Akshay Naik, and Marc Manheimer are gratefully acknowledged. E.K.I. acknowledges support from the National Physical Sciences Consortium.

\*

### APPENDIX A: DERIVATION OF THE EFFECTIVE CPB HAMILTONIAN

The Hamiltonian for the Cooper-pair box in the basis of charge states is<sup>29</sup>

$$H_{CPB} = -4E_C(\frac{1}{2} - n_g)\hat{\sigma}_z - \frac{1}{2}E_J\hat{\sigma}_x, \quad (A1)$$

where  $\hat{\sigma}_z, \hat{\sigma}_x$  are Pauli spin matrices operating in the charge basis of the CPB;  $n_g = C_b V_b / 2e$  where  $C_b$  and  $V_b$  are the CPB biasing capacitance and voltage; and  $E_C$  and  $E_J$  are the Coulomb and Josephson energies. Eq. (A1) may also be written in terms of the mixing angle  $\eta \equiv \tan^{-1}\{E_J/[8E_C(1/2 - n_g)]\}$ :

$$H_{CPB} = -\frac{1}{2}\Delta E(\eta)(\cos \eta \hat{\sigma}_z + \sin \eta \hat{\sigma}_x), \quad (A2)$$

where  $\Delta E(\eta) = \sqrt{[8E_C(1/2 - n_g)]^2 + E_J^2}$ . Alternatively, the Hamiltonian may be written in the diagonal form

$$\tilde{H}_{CPB} = -\frac{1}{2}\Delta E(\eta)\hat{\rho}_z \quad (A3)$$

where the Pauli operators which operate in the eigenbasis of  $H_{CPB}$  are defined as

$$\hat{\rho}_z \equiv \cos \eta \hat{\sigma}_z + \sin \eta \hat{\sigma}_x \quad (A4)$$

$$\hat{\rho}_x \equiv \cos \eta \hat{\sigma}_x - \sin \eta \hat{\sigma}_z \quad (A5)$$

$$\hat{\rho}_y \equiv \hat{\sigma}_y. \quad (A6)$$

An oscillating voltage  $V_b^{ac}$  may be applied to the bias gate of the CPB, resulting in an additional term in the Hamiltonian<sup>26</sup>  $H_{ac} = \hbar g \cos(\omega t)\hat{\sigma}_z$  where  $g = 4E_C C_b V_b^{ac} / 2e\hbar$ . In the eigenbasis of  $H_{CPB}$  this becomes

$$\tilde{H}_{ac} = \frac{1}{2}\hbar g(e^{i\omega t} + e^{-i\omega t})[\cos \eta \hat{\rho}_z - \sin \eta(\hat{\rho}_+ + \hat{\rho}_-)], \quad (A7)$$

where  $\hat{\rho}_\pm = \frac{1}{2}(\hat{\rho}_x \pm i\hat{\rho}_y)$  are raising (lowering) operators for the CPB.

We will assume that  $\omega \approx \Delta E(\eta)/\hbar$  so that the rotating wave approximation may be used to derive a time-independent effective Hamiltonian for the CPB with oscillating bias voltage. The first step is to transform into a reference frame which is rotating about the  $\hat{\rho}_z$  axis at the frequency  $\omega$ . This may be accomplished by the transformation

$\tilde{H}_{rot} = \hat{U}^\dagger \tilde{H} \hat{U} - i\hbar \hat{U}^\dagger d\hat{U}/dt$  with  $\hat{U} = \exp(i\omega t \hat{\rho}_z/2)$ . Noting that  $\hat{U}^\dagger \hat{\rho}_\pm \hat{U} = \exp(\mp i\omega t) \hat{\rho}_\pm$ , the Hamiltonian  $\tilde{H}_{CPB} + \tilde{H}_{ac}$  transforms to

$$\tilde{H}_{rot} = -\frac{1}{2}\hbar\Delta\hat{\rho}_z + \frac{1}{2}\hbar g(e^{i\omega t} + e^{-i\omega t}) \cos\eta\hat{\rho}_z - \frac{1}{2}\hbar g \sin\eta(\hat{\rho}_+ + \hat{\rho}_- + e^{-2i\omega t}\hat{\rho}_+ + e^{2i\omega t}\hat{\rho}_-) \quad (\text{A8})$$

where  $\Delta \equiv \Delta E(\eta)/\hbar - \omega$  is the detuning between the CPB splitting frequency and the frequency of the oscillating bias voltage. As long as we are interested in motion on the timescale of  $g \ll \omega$ , the time-dependent terms in Eq. (A8) may be neglected. With this approximation, and transforming back to the charge basis, we obtain

$$H_{CPB} \approx -\frac{1}{2}\hbar\Delta(\cos\eta\hat{\sigma}_z + \sin\eta\hat{\sigma}_x) - \frac{1}{2}\hbar g \sin\eta(\cos\eta\hat{\sigma}_x - \sin\eta\hat{\sigma}_z). \quad (\text{A9})$$

If we assume the CPB to be biased far from degeneracy such that  $\sin\eta \ll \cos\eta$  and take the detuning  $\Delta = 0$ , we find an effective Hamiltonian for the CPB<sup>31</sup>

$$H_{CPB}^{eff} = -\frac{1}{2}\hbar\Omega\hat{\sigma}_x \quad (\text{A10})$$

where  $\Omega \equiv g \sin\eta \cos\eta$ . The Hamiltonians for the NR and the interaction between the CPB and NR remain as given in Eq. (24). Combining these terms yields a Hamiltonian for the coupled system of the form of Eq. (1).

---

\* Electronic address: eirish@lps.umd.edu

<sup>1</sup> E. T. Jaynes and F. W. Cummings, Proc. IEEE **51**, 89 (1963).

<sup>2</sup> J. M. Raimond, M. Brune, and S. Haroche, Rev. Mod. Phys. **73**, 565 (2001).

<sup>3</sup> C. J. Hood, T. W. Lynn, A. C. Doherty, A. S. Parkins, and H. J. Kimble, Science **287**, 1447 (2000).

<sup>4</sup> A. Wallraff, D. I. Schuster, A. Blais, L. Frunzio, R.-S. Huang, J. Majer, S. Kumar, S. M. Girvin, and R. J. Schoelkopf, Nature **431**, 162 (2004).

<sup>5</sup> I. Chiorescu, P. Bertet, K. Semba, Y. Nakamura, C. J. P. M. Harmans, and J. E. Mooij, Nature **431**, 159 (2004).

<sup>6</sup> A. D. Armour, M. P. Blencowe, and K. C. Schwab, Physica B **316-317**, 406 (2002).

<sup>7</sup> A. D. Armour, M. P. Blencowe, and K. C. Schwab, Phys. Rev. Lett. **88**, 148301 (2002).

<sup>8</sup> E. K. Irish and K. Schwab, Phys. Rev. B **68**, 155311 (2003).

<sup>9</sup> B. W. Shore and P. L. Knight, J. Mod. Optics **40**, 1195 (1993).

<sup>10</sup> R. Graham and M. Höhnerbach, Z. Phys. B: Condens. Matter **57**, 233 (1984).

<sup>11</sup> R. Graham and M. Höhnerbach, Acta Phys. Austriaca **56**, 45 (1984).

<sup>12</sup> R. Graham and M. Höhnerbach, Phys. Lett. A **101**, 61 (1984).

<sup>13</sup> S. Schweber, Ann. Phys. (N.Y.) **41**, 205 (1967).

<sup>14</sup> M. D. Crisp, Phys. Rev. A **46**, 4138 (1992).

<sup>15</sup> L. Mandel and E. Wolf, *Optical Coherence and Quantum Optics* (Cambridge University Press, Cambridge, 1995).

<sup>16</sup> A. J. Leggett, S. Chakravarty, A. T. Dorsey, M. P. A. Fisher, A. Garg, and W. Zwerger, Rev. Mod. Phys. **59**, 1 (1987).

<sup>17</sup> D. H. Santamore, A. C. Doherty, and M. C. Cross, Phys. Rev. B **70**, 144301 (2004).

<sup>18</sup> M. D. LaHaye, O. Buu, B. Camarota, and K. C. Schwab, Science **304**, 74 (2004).

<sup>19</sup> F. W. Cummings, Phys. Rev. **140**, A1051 (1965).

<sup>20</sup> J. H. Eberly, N. B. Narozhny, and J. J. Sanchez-Mondragon, Phys. Rev. Lett. **44**, 1323 (1980).

<sup>21</sup> P. L. Knight and P. M. Radmore, Phys. Lett. A **90**, 342 (1982).

<sup>22</sup> N. B. Narozhny, J. J. Sanchez-Mondragon, and J. H. Eberly, Phys. Rev. A **23**, 236 (1981).

<sup>23</sup> M. Abramowitz and I. A. Stegun, eds., *Handbook of Mathematical Functions* (Dover Publications, New York, 1970).

<sup>24</sup> P. L. Knight, Phys. Scr. **T12**, 51 (1986).

<sup>25</sup> X. M. H. Huang, C. A. Zorman, M. Mehregany, and M. L. Roukes, Nature (London) **421**, 496 (2003).

<sup>26</sup> K. W. Lehnert, K. Bladh, L. F. Spietz, D. Gunnarsson, D. I. Schuster, P. Delsing, and R. J. Schoelkopf, Phys. Rev. Lett. **90**, 027002 (2003).

<sup>27</sup> D. Vion, A. Aassime, A. Cottet, P. Joyez, H. Pothier, C. Urbina, D. Esteve, and M. H. Devoret, Science **296**, 886 (2002).

<sup>28</sup> T. Duty, D. Gunnarsson, K. Bladh, and P. Delsing, Phys. Rev. B **69**, 140503(R) (2004).

<sup>29</sup> Y. Makhlin, G. Schön, and A. Shnirman, Rev. Mod. Phys. **73**, 357 (2001).

<sup>30</sup> It may be interesting to note that  $\Omega'^{(0)}$  may be obtained from Eq. (3.20) of Ref. 16 by setting the spectral density  $J(\omega) = \delta(\omega - \omega_0)$ : that is, by treating the NR as a single-mode bath causing decoherence of the CPB.

<sup>31</sup> For the sake of simplicity, the effective Hamiltonian is left in the rotating frame. The effect on the expectation value of  $\hat{\sigma}_z$ , which is all we consider in this paper, is negligible within the assumptions we have already made.